# Phase transitions and vortex-line entanglement in a model high-temperature superconductor

Ying-Hong Li*
*Institute for Theoretical Physics, University of Utrecht, P.O. Box 80.006, 3508 TA Utrecht, The Netherlands*

S. Teitel
*Department of Physics and Astronomy, University of Rochester, Rochester, New York 14627*
(Received 29 July 1993)

We carry out Monte Carlo simulations of the uniformly frustrated three-dimensional $XY$ model, as a model for vortex-line fluctuations in high-temperature superconductors in an applied magnetic field. We show, comparing systems of different size, that there are two distinct phase transitions. At a lower $T_{c\perp}$, the vortex lattice melts, and coherence is lost in planes perpendicular to the magnetic field. At a higher $T_{cz}$, a vortex tangle percolates throughout the system, and coherence is lost parallel to the magnetic field. Cooling below $T_{cz}$, high-energy barriers for vortex-line cutting lead to an entangled glassy state.

## I. INTRODUCTION

In several earlier works[1,2] we introduced the three-dimensional uniformly frustrated $XY$ model,[3] as a phenomenological model for studying phase transitions, and the effects of vortex-line fluctuations, in the mixed state of high-temperature superconductors in a uniform applied magnetic field. This model applies in the strongly type-II limit where the magnetic penetration length is much greater than the average vortex-line separation, $\lambda \gg a_v$, and the magnetic induction inside the superconductor is approximately uniform. In our most recent work,[2] henceforth referred to as (I), we found evidence that the system undergoes two distinct phase transitions upon heating. First, at the lower $T_{c\perp}$, the vortex-line lattice melts, destroying superconducting phase coherence in directions perpendicular to the applied magnetic field; coherence parallel to the field however remains. Then, at the higher $T_{cz}$, coherence parallel to the field is lost as well.

In the present work we extend the results of (I) in several major directions: (i) By presenting detailed studies of the system behavior as the system size is varied in the directions parallel and perpendicular to the magnetic field, we show clearly that the two distinct transitions found in (I) are not artifacts of finite size effects. (ii) We show that the upper transition $T_{cz}$ can be viewed as a percolationlike transition, where the vortex lines become so completely interconnected through mutual intersections that one may trace out a connected path of vortex-line segments which travels completely around the system in the direction *perpendicular* to the applied magnetic field. (iii) We find, in contrast to our earlier results, that below $T_{cz}$ the energy barrier for vortex-line cutting grows so large that cuttings are frozen out on the time scale of our simulation, and the system can cool into an entangled glassy state as in the "polymer glass" picture originally proposed by Nelson[4] and further studied by Obukhov and Rubinstein.[5]

The remainder of our paper is organized as follows. In Sec. II we outline our model and Monte Carlo method. In Sec. III we present the results of our simulations. Section III A gives results for the helicity modulus, which measures superconducting phase coherence. Section III B gives results for the average length of vortex lines due to thermal fluctuations. Section III C analyzes the entanglement of the vortex lines by considering the winding of the field induced vortex lines about the direction of the magnetic field. Finite size dependences are investigated. Section III D gives results concerning the distribution of thermally excited closed vortex rings. Section III E discusses the "two-dimensional (2D) boson" analogue to vortex-line fluctuations, as applied to our model. In Sec. IV we summarize our results and discuss the possible connection to recent experiments.

## II. MODEL

The model that we study is given by the Hamiltonian[2]

$$\mathcal{H}[\theta_i] = J_0 \sum_{\langle ij \rangle} V(\theta_i - \theta_j - A_{ij}), \tag{1}$$

where $\theta_i$ is the phase of the superconducting wave function at site $i$ of a three-dimensional cubic numerical mesh, the sum is over all nearest neighbor bonds of this mesh,

$$A_{ij} = \frac{2\pi}{\Phi_0} \int_i^j \mathbf{A} \cdot d\boldsymbol{l} \tag{2}$$

is proportional to the integral of the fixed magnetic vector potential $\mathbf{A}$ across bond $\langle ij \rangle$ ($\Phi_0 = hc/2e$ is the flux quantum),

$$V(\alpha) \equiv -(T/J_0) \ln \left\{ \sum_{m=-\infty}^{\infty} \exp\left[ -\frac{1}{2} J_0 (\alpha - 2\pi m)^2 / T \right] \right\} \tag{3}$$

 

is the Villain interaction between neighboring sites, and the coupling is

$$J_0 = \frac{\Phi_0^2 \xi_0}{16\pi^3 \lambda^2}, \tag{4}$$

where we identify the vortex core radius $\xi_0$ with the lattice constant $a$ of our numerical mesh. For our numerical studies we take an isotropic uniform constant $J_0$, although this could be varied if desired to model the effects of anisotropy or randomness. Periodic boundary conditions are chosen in all directions.[6] Numerical meshes of various sizes $L_\perp^2 \times L_z$ are studied (the subscript "$\perp$" will refer to the $\hat{\mathbf{x}}$ and $\hat{\mathbf{y}}$ directions, transverse to the applied magnetic field).

The approximations which lead from the familiar Landau-Ginzburg free energy functional to the Hamiltonian (1), and their justifications in the $\lambda \gg a_v$ limit, have been described in detail in (I). In the following, we study the specific case where the uniform magnetic induction $\mathbf{B} = \nabla \times \mathbf{A}$ is $f = 1/25$ flux quantum per plaquette of the mesh, oriented in the $\hat{\mathbf{z}}$ direction. The ground state is a square periodic lattice of straight magnetic field induced vortex lines with spacing $a_v/a = 1/\sqrt{f} = 5$, as shown in Fig. 1. Henceforth, we cite all lengths in units of $a \simeq \xi_0$, and energies in units of $J_0$. The total number of field induced lines is $N_v = f L_\perp^2$.

Our Monte Carlo simulations are carried out using the standard Metropolis algorithm. Performing the simulation in terms of the phase variables $\theta_i$, we locate the vortex lines in any particular configuration by computing the net phase change around every plaquette of the mesh. We define as an intersection, or cutting, between two vortex lines whenever we find a unit cell of the mesh which has more than one vortex line entering and leaving. In such a situation, we randomly assign which exiting segment is connected to which entering segment, for the purpose of identifying the paths of these particular lines. Each of our data points is typically the result of 2000 sweeps to equilibrate, followed by 15 000 sweeps to compute averages, where each sweep refers to one updating pass through the entire numerical mesh. Our calculations were carried out on a Sparc 10 workstation; for our largest system, $25^2 \times 200$, each temperature point took approximately 2 CPU days of computation.

## III. RESULTS

### A. Helicity modulus

To investigate phase coherence, we compute the helicity moduli, which give the stiffness of the system to twisted phase boundary conditions [see (I) for derivation]. In Fig. 2 we show our results for the helicity modulus $\Upsilon_\perp(T)$ perpendicular to the magnetic field, and $\Upsilon_z(T)$ parallel to the magnetic field, for lattices of fixed size $L_\perp = 25$, but varying $L_z = 50$, 100, and 200. In Fig. 3 we show $\Upsilon_\perp(T)$ and $\Upsilon_z(T)$ for approximately equal $L_z = 24$, 25, but varying $L_\perp = 25$ and 50. We see clearly two transitions, with $\Upsilon_\perp$ vanishing at $T_{c\perp} \simeq 1.35$, and $\Upsilon_z$ vanishing at $T_{cz} \simeq 2.6$. Comparing the results from different $L_\perp$ and $L_z$, finite size effects are generally seen to be small; hence we have clear evidence for three distinct thermodynamic states. The middle state is one in which superconducting phase coherence is destroyed in planes perpendicular to the magnetic field, but coherence is preserved in the direction parallel to the magnetic field. Comparing the results for heating versus cooling, we see only a small hysteresis in $\Upsilon_z$; however, hysteresis in $\Upsilon_\perp$ increases with increasing $L_z$. We will see that this hysteresis in $\Upsilon_\perp$ is related to the entanglement of the vortex lines as they cool into a glassy state.

### B. Vortex-line lengths

As a first measure of the amount and nature of vortex-line fluctuations, we consider the average density

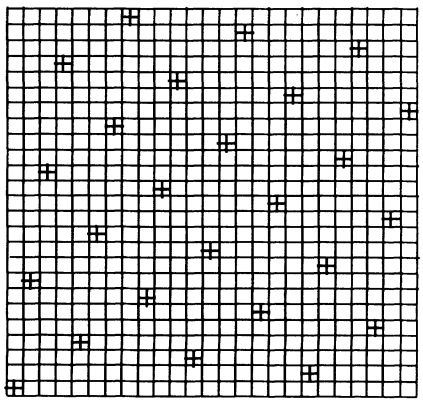

FIG. 1. Ground-state vortex-line lattice for a magnetic induction of $f = B\xi_0^2/\Phi_0 = 1/25$ flux quantum per unit cell of the numerical mesh. The view is along the direction of $\mathbf{B}$ and (+) locates the positions of the straight vortex lines.

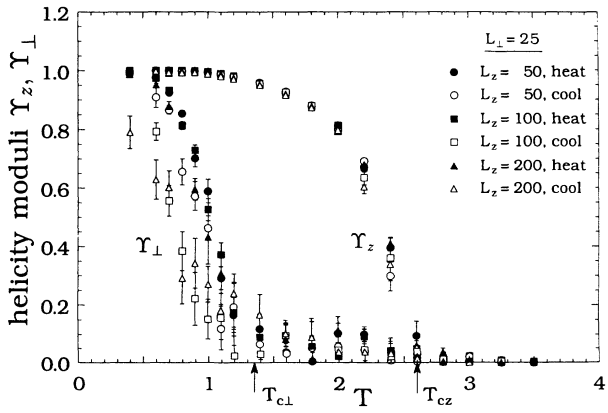


FIG. 2. Helicity modulus $\Upsilon_z$ along the direction of $\mathbf{B}$, and $\Upsilon_\perp$ perpendicular to $\mathbf{B}$, for lattice sizes $L_\perp = 25$ and varying $L_z = 50$, 100, and 200. Both heating and cooling are shown. The vanishing of $\Upsilon_{z,\perp}$ indicates two separate transitions. No significant finite size effects are seen.

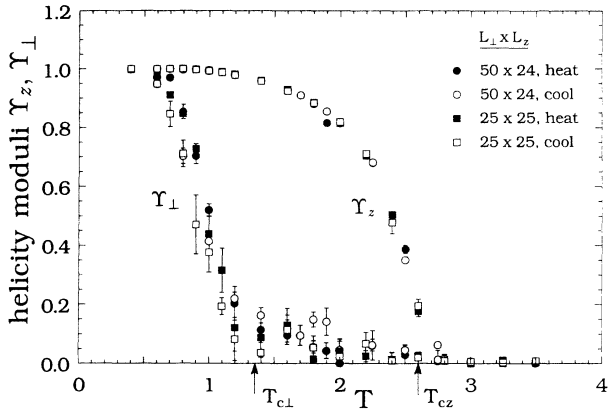


FIG. 3. Helicity modulus $\Upsilon_z$ along the direction of $\mathbf{B}$, and $\Upsilon_\perp$ perpendicular to $\mathbf{B}$, for lattice sizes $L_z = 25$, $L_\perp = 25$ and $L_z = 24$, $L_\perp = 50$. Both heating and cooling are shown. No significant finite size effects are seen.

of vortex-line segments in different directions. In the ground state, the total length of vortex-lines is $N_v L_z$ along $\hat{\mathbf{z}}$, while zero along $\hat{\mathbf{x}}$ and $\hat{\mathbf{y}}$. In Fig. 4 we plot the vortex-line length density $\Delta l_\mu$ versus temperature, where $\Delta l_\mu$ is defined as the total length of vortex-line segments due to fluctuations (i.e., in excess over the ground state value) in direction $\hat{\boldsymbol{\mu}}$, normalized by $N_v L_z$. $\Delta l_\mu = 1$ represents an excess vortex-line length equal to that of the straight field induced lines at $T = 0$. We see that $\Delta l_{x,y} \gg \Delta l_z$ in the vortex-line lattice phase below $T_{c\perp}$, as well as for much of the vortex-line liquid phase between $T_{c\perp}$ and $T_{cz}$. This indicates that in these regions, the dominant fluctuations are directed transverse fluctuations of the magnetic field induced vortex lines, as shown schematically in Fig. 5(a). Near and above $T_{cz}$, however,

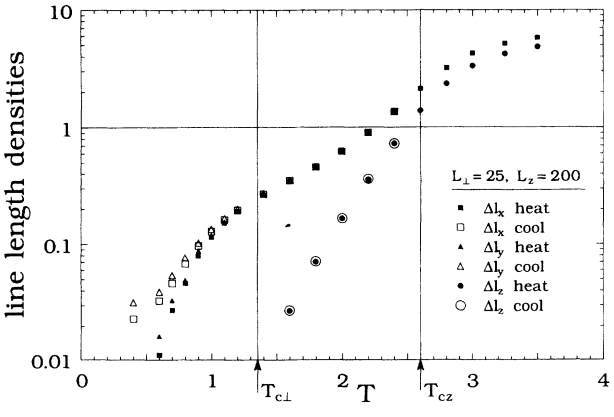


FIG. 4. Line length densities $\Delta l_\mu$, measuring absolute value of total vortex-line lengths in direction $\hat{\boldsymbol{\mu}}$, normalized by total length in ground-state $N_v L_z$. For $\Delta l_z$, the ground-state line length has been subtracted, in order to show only excess length due to fluctuations. Both heating and cooling are shown for a fixed lattice size $L_\perp = 25$, $L_z = 200$. The solid horizontal line indicates the total normalized length in the ground state; the solid vertical lines mark the transition temperatures as obtained from the vanishing of $\Upsilon_{z,\perp}$.

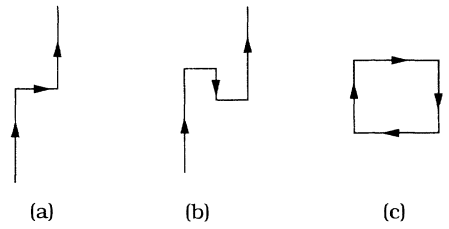


FIG. 5. Schematic of possible vortex fluctuations. (a) shows a directed fluctuation of a field induced vortex line; the line pierces each plane of constant $z$ only once. (b) shows a field induced vortex line with an overhang. (c) shows a closed vortex ring excitation.

we find that $\Delta l_{x,y} \simeq \Delta l_z$. We will see that this is due to the proliferation of closed vortex ring excitations as shown in Fig. 5(c). Above $T_{cz}$, $\Delta l_\mu > 1$, and the total vorticity is dominated by the contribution from fluctuations. We will see that this region is an interconnected tangle of vortex-line segments, with no unambiguous separation between field induced lines and thermally excited rings.

### C. Entanglement

To consider the entanglement of the field induced vortex lines, we make use of the periodic boundary condition which is imposed along the direction of the magnetic field $\hat{\mathbf{z}}$. If $\{\mathbf{r}_{\perp i}(z)\}$ are the positions in the $xy$ plane where the field induced vortex lines intersect the plane at constant $z$, then the set of points $\{\mathbf{r}_{\perp i}(0)\}$ must be identical to the set of points $\{\mathbf{r}_{\perp i}(L_z)\}$. If we view this periodic boundary condition along $\hat{\mathbf{z}}$ as representing the circumference of a three-dimensional torus, then the magnetic field induced vortex lines will divide into distinct connected groups, each of which makes a certain number of windings around the system in the $\hat{\mathbf{z}}$ direction before closing back on itself. A group making a winding $m$ would consist of the $m$ lines $i_1, i_2, ..., i_m$ satisfying the condition $\mathbf{r}_{\perp i_1}(0) = \mathbf{r}_{\perp i_2}(L_z)$, $\mathbf{r}_{\perp i_2}(0) = \mathbf{r}_{\perp i_3}(L_z)$, ..., $\mathbf{r}_{\perp i_m}(0) = \mathbf{r}_{\perp i_1}(L_z)$. For example, in Fig. 6, we show a configuration with two lines of

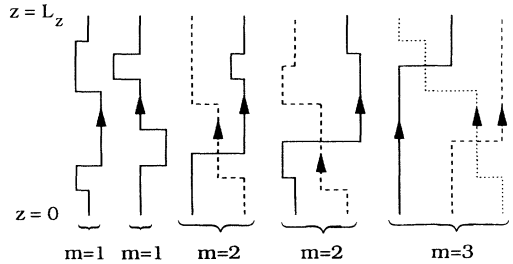


FIG. 6. Schematic of possible reconnections of field induced vortex lines, under application of the periodic boundary condition in the $\hat{\mathbf{z}}$ direction. This example shows two lines of winding $m = 1$, two groups of lines with winding $m = 2$, and one group of lines with winding $m = 3$. Solid, dashed, and dotted lines are use to distinguish the different lines within a particular winding group.

winding $m = 1$, two groups of lines with winding $m = 2$, and one group of lines with winding $m = 3$. Qualitatively, when a configuration contains only windings with $m = 1$, we say that it is "unentangled." When a configuration contains many windings with large values of $m$, it is highly entangled. To characterize the degree of entanglement, we compute the average distribution $n(m)$ of the total number of lines $n$ which participate in windings of value $m$: $\sum_m n(m) = N_v$, the total number of field induced vortex lines.

In Fig. 7 we plot versus $T$ for several different system sizes, the ratio $R \equiv n(1)/N_v$ of lines which make a winding of $m = 1$. $R = 1$ indicates a completely unentangled set of lines. We see that for all sizes upon *heating* from the ground state, $R \simeq 1$ stays constant until about $T \simeq 2.0 > T_{c\perp}$, then decreases to its high $T$ limit at $T_{cz}$. Upon *cooling*, however, $R$ starts to rise below $T_{cz}$ and saturates around $T_{c\perp}$ to a value $R \leq 1$, dependent on system size. Only for our shortest system, $L_z = 50$, do we find disentanglement, i.e., $R = 1$ upon cooling. For all larger $L_z$, the lines remain trapped in a nonequilibrium entangled state upon cooling [in (I) our system size was $L_z = 24$; hence we failed to see the entanglement below $T_{cz}$ that we now find]. The degree of this entanglement increases (i.e., $R$ decreases) with increasing $L_z$. As this cooled state is not in equilibrium, it is unclear if the low-temperature value of $R$ may vary with independent coolings, or if it may strongly depend on the rate of cooling. To test this, we have carried out four independent coolings of the system size $L_\perp = 25$, $L_z = 100$, and find the $T \to 0$ values of $R = 0.64$, 0.68, 0.75, and 0.79. The second of these coolings was carried out using twice the number of Monte Carlo sweeps per temperature as for the rest of our data. We similarly have carried out four independent coolings of the system size $L_\perp = 15$, $L_z = 100$, finding values of $R(T \to 0) = 0.44$, 1.0, 0.41, and 0.38. The second run indicates that large fluctuations in $R$ are possible.

The strong hysteresis we find in $R$, which measures the global topology of the lines, should be contrasted with the absence of hysteresis in the line length densities $\Delta l_\mu$ (see Fig. 4), which are a local measure of line fluctuations (the slight hysteresis in $\Delta l_{x,y}$ which appears below $T \simeq 1.0 < T_{c\perp}$ is due to the extra geometrical line length needed to make a quenched entangled state, compared to a lattice of straight lines). This suggests that the hysteresis in $R$ is due to the energy barrier for the cutting of vortex lines. As $T$ decreases below $T_{cz}$, thermal activation over this energy barrier, which is necessary to disentangle the lines, becomes frozen out on the times scales of our simulation. As a measure of this energy barrier, we compute the average number of line cuttings $N_c$ (unit cells with more than one line entering and leaving) present in the system. We then define the cutting length $\xi_c \equiv N_v L_z / N_c$ as the average distance in the $\hat{\mathbf{z}}$ direction between two successive cuttings of a single line. We plot $\xi_c$ versus $T$ in Fig. 8. Above $T_{cz}$ we find $\xi_c \simeq 1$–2 indicating a heavily interconnected tangle of lines with much cutting. As $T$ decreases below $T_{cz}$, $\xi_c$ increases rapidly, becoming of the order of $L_z$. The absence of any size dependence in $\xi_c$ comparing the system with $L_z = 50$ (which disentangles upon cooling) versus $L_z = 200$ (which remains entangled upon cooling) suggests that much of the cutting which determines $\xi_c$ in the region below $T \simeq 2.0$ may be due to the intersection between field induced lines and thermally excited closed vortex rings, rather than between two field induced lines; cuttings between field induced lines may only be occurring on even larger length scales. This picture we find of cooling into a nonequilibrium entangled state is therefore similar to the "polymer glass" transition[4,5] originally proposed by Nelson. Comparing the data for $L_z = 50$ with $L_z = 200$ in Fig. 2, it is interesting to note that with respect to phase coherence, entanglement has a noticeable effect only on the helicity modulus $\Upsilon_\perp$; $\Upsilon_z$ seems entirely unaffected.

As a further measure of the process of vortex line entanglement, we now consider the complete distribution of line windings $n(m)$. In Fig. 9 we show $n(m)$, for a fixed system size of $L_\perp = 25$, $L_z = 200$, for various tempera-

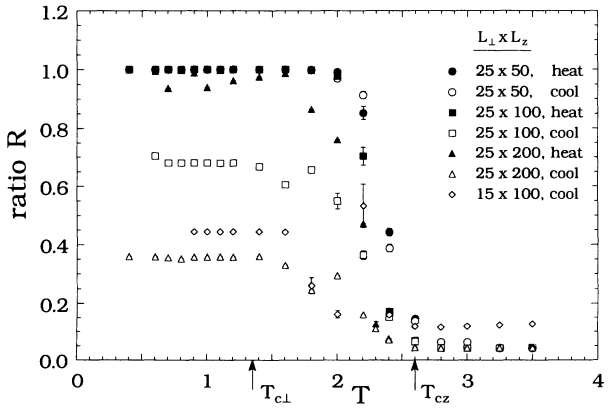


FIG. 7. Fraction of field induced vortex lines which are unentangled, $R \equiv n(1)/N_v$, for various system sizes. Note the strong hysteresis between cooling and heating. Entanglement increases as $L_z$ increases.

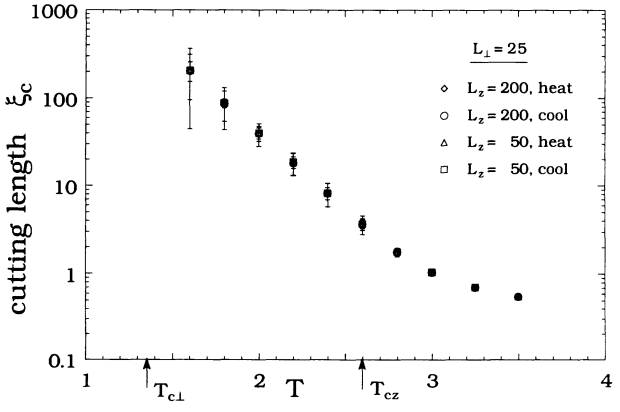


FIG. 8. Distance $\xi_c$ along $\hat{\mathbf{z}}$ between two successive cuttings of a single field induced vortex line. $\xi_c \sim 1$–2 for $T > T_{cz}$ indicates a heavily interconnected vortex tangle.

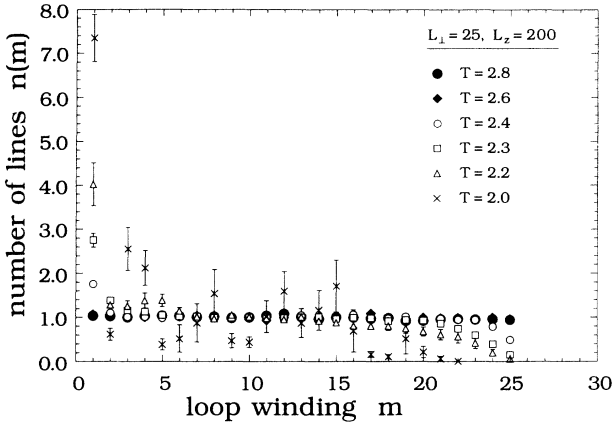


FIG. 9. Distribution of windings $n(m)$ that field induced vortex lines make in traveling around the system along the $\hat{\mathbf{z}}$ direction. Several different temperatures are shown for the fixed system size $L_\perp = 25$, $L_z = 200$. For $T > T_{cz} \simeq 2.6$, we find $n(m) \equiv 1$.

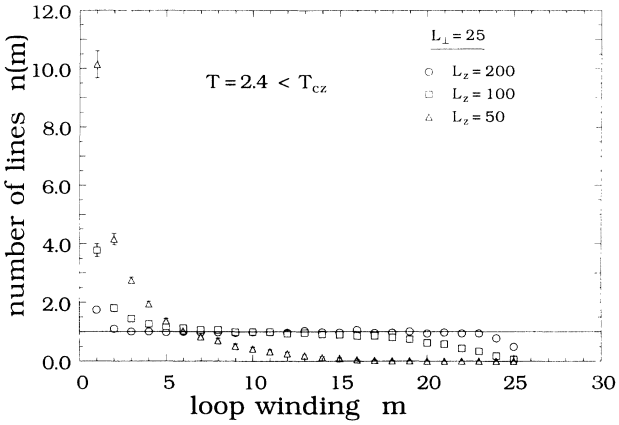


FIG. 10. Distribution of windings $n(m)$ for fixed $T = 2.4 < T_{cz}$, for system sizes $L_\perp = 25$ and $L_z = 50$, 100, 200. As $L_z$ increases, $n(m) \to 1$; i.e., entanglement increases.

tures. The results shown were obtained upon cooling the system. We find that for all $T \geq T_{cz} \simeq 2.6$, the distribution is $n(m) = 1$ for all $m$; i.e., a field induced vortex line selected at random is equally likely to belong to a winding of any value $m$. This result is consistent with the assumption that each vortex line $i$ is equally likely to reconnect onto any other vortex line $j$, upon traversing the system in the $\hat{\mathbf{z}}$ direction once; i.e., $\mathbf{r}_{\perp i}(0) = \mathbf{r}_{\perp j}(L_z)$ is equally likely for any $i$ and $j$. The most likely explanation for such behavior is that above $T_{cz}$ the lines become so completely interconnected due to cuttings that the global path of a given line is primarily determined by our algorithm which makes a random choice for the continuation of the line at each individual cutting. When each line has sufficient cuttings with its neighbors, the resulting line path our algorithm traces out is equally likely to meander anywhere throughout the system. This conclusion is supported by Fig. 8 where we see $\xi_c \simeq 1$–2 for $T \geq T_{cz}$. We will see further evidence for this later when we consider the distribution of thermally excited vortex rings.

As $T$ decreases below $T_{cz}$ in Fig. 9, we find a steady increase in $n(m)$ at smaller $m$, compensated by a decrease in $n(m)$ at the largest $m$. This is as one would expect when the connectivity of any pair of field induced vortex lines $i$ and $j$, i.e., $\mathbf{r}_{\perp i}(0) = \mathbf{r}_{\perp j}(L_z)$, becomes dominated by the thermal transverse wandering of the lines as they pass through the system along $\hat{\mathbf{z}}$, rather than by line cuttings. As $T$ decreases, the transverse wandering decreases, and the probability for near neighbor reconnections increases with the resulting increase in $n(m)$ for small $m$. It is interesting to note, however, that even for $T$ moderately below $T_{cz}$, there remains a wide region of intermediate $m$, where we continue to find $n(m) \simeq 1$. For $T = 2.3$–2.6 we believe that, even though we are below $T_{cz}$, the energy barrier for line cutting is still sufficiently small compared to $T$ that our data represent true equilibrium behavior (see $\xi_c \leq 10$ in Fig. 8, and the absence of hysteresis in $R$ in Fig. 7, for these values of $T$). As $T$ is cooled below $\sim 2.3$, the system gets trapped in some random metastable nonequilibrium tangle.

We now consider the finite size dependence of entanglement. In Fig. reffig10(c) we plot $n(m)$ for systems of fixed $L_\perp$, but varying $L_z = 50$, 100, and 200. Our data is for the fixed temperature $T = 2.4$, below $T_{cz}$, yet still high enough that we are sampling equilibrium. We see that as $L_z$ increases, $n(m)$ approaches the $T > T_{cz}$ limit of unity. This may be understood as a result of the increased transverse wandering of lines as $L_z$ increases, thus decreasing the probability of neighboring pair reconnections. Considering the value of $n(1)$, we see that it decreases by a factor $\sim 2$ as $L_z$ increases from 100 to 200, consistent with a random-walk-like behavior for the vortex-line transverse fluctuations. This leads one to expect that in the limit $L_z \to \infty$, for fixed $L_\perp$, the system will remain completely entangled at all $T < T_{cz}$.

In Fig. 11 we plot $n(m)$ at $T = 2.4$ for systems of fixed $L_z = 100$, but varying $L_\perp = 15$, 20, and 25. These are systems with a total of $N_v = 9$, 16, and 25 field induced

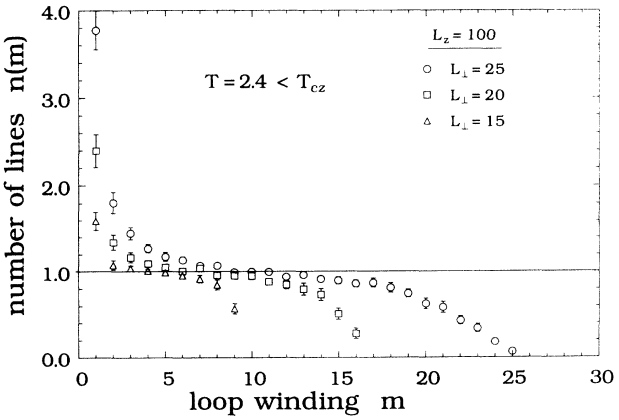


FIG. 11. Distribution of windings $n(m)$ for fixed $T = 2.4 < T_{cz}$, for system sizes $L_z = 100$ and $L_\perp = 15$, 20, 25. Distribution remains flat, $n(m) \simeq 1$, for wide region of intermediate $m$ as $L_\perp$ increases.

vortex lines, respectively. As the maximum winding is always $m_{\max} = N_v$, the falloff of $n(m)$ at large $m$ occurs at different $m \sim N_v$ for the different $L_\perp$. If we normalize the different curves in Fig. 11 by $N_v$ [recall, $\sum_m n(m) = N_v$], we find that $R \equiv n(1)/N_v$ is approaching a constant value as $L_\perp \to \infty$ (see also Fig. 7). Thus the fraction of disentangled lines is approaching a well-defined value. However, we show the curves without this normalization to point up the wide intermediate region where we continue to find $n(m) \sim 1$ as $L_\perp$ increases. These observations suggest that for $T < T_{cz}$ for fixed $L_z$, as $L_\perp$ increases, the equilibrium probability distribution of windings $n(m)/N_v$ approaches a limiting form, but the average value of $m$ diverges.

### D. Vortex ring excitations

We now consider the proliferation of thermally excited closed vortex ring excitations as illustrated in Fig. 5(c). Defining $q(p)$ as the total number of vortex rings with perimeter $p$, we plot in Fig. 12 the logarithm of $q(p)$ versus $1/T$, for $p = 2, \ldots, 40$. Our data is for the system size $L_z = 100$, $L_\perp = 25$. We show the results obtained from cooling; comparison with data from heating shows no significant hysteresis. For $T < T_{cz}$ the data fall along straight lines over several orders of magnitude, clearly indicating a thermally activated form. These lines intersect at roughly the same temperature, $1/T_0 \simeq 0.3$, thus suggesting the low-temperature form

$$q(p) \simeq q_0 e^{-E(p)(1/T - 1/T_0)}. \tag{5}$$

In Fig. 13 we plot the value of $E(p)$, extracted from the data of Fig. 12, versus $p$ and find the linear dependence

$$E(p) = -1.14 + \varepsilon p, \qquad \varepsilon = 3.32. \tag{6}$$

Thus for $T < T_{cz}$, the number of rings $q(p)$ is determined by the excitation energy to create the ring, and this energy scales linearly with the ring perimeter. As $T$ decreases, large rings get exponentially suppressed.

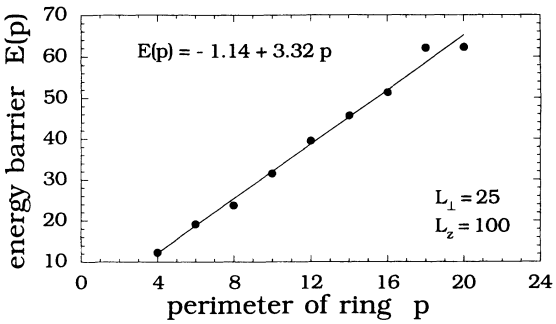


FIG. 13. Energy barrier $E(p)$ for vortex rings of perimeter $p$, as extracted from the $T < T_{cz}$ data of Fig. 12. $E(p)$ scales linearly with $p$.

For $T > T_{cz}$, we see from Fig. 12 that $q(p)$ saturates to a constant value, and that rings on all length scales $p$ are now present. As discussed above in connection with the winding distribution $n(m)$, we believe that this saturation of $q(p)$ is the result of a transition in which the vortex lines become so heavily interconnected through cuttings that a connected vortex tangle percolates through the entire system. In this heavily interconnected limit, there is in general no unambiguous way to classify a given vortex-line segment as belonging to a particular ring of size $p$, or even as belonging to a ring versus a field induced line. The distribution $q(p)$ would then be dominated by the statistics of our line tracing algorithm which makes random choices at each line cutting, rather than by any energetics.

In Fig. 14 we replot our data as $q(p)$ versus $p$ for several different $T$. We show only data for sizes $p$ in which the finite size effects, comparing different $L_\perp = 15$, 20, 25, are small [to determine these finite size effects, we compared the *normalized* ring densities $q(p)/L_z L_\perp^2$].

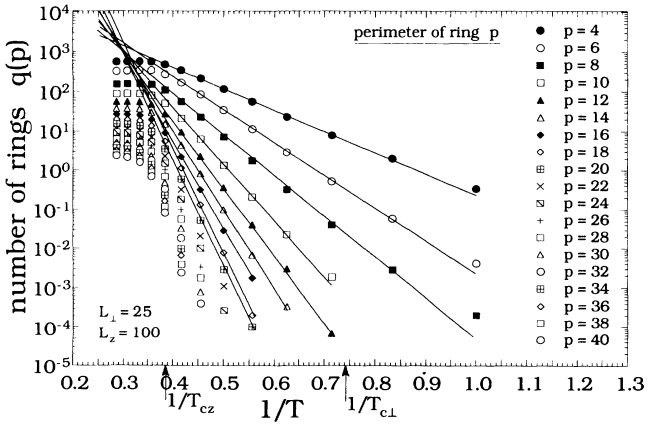


FIG. 12. Distribution of thermally excited closed vortex rings of perimeter $p$ versus $1/T$ for fixed system size $L_\perp = 25$, $L_z = 100$. Straight solid lines for $T < T_{cz}$ show thermally activated behavior.

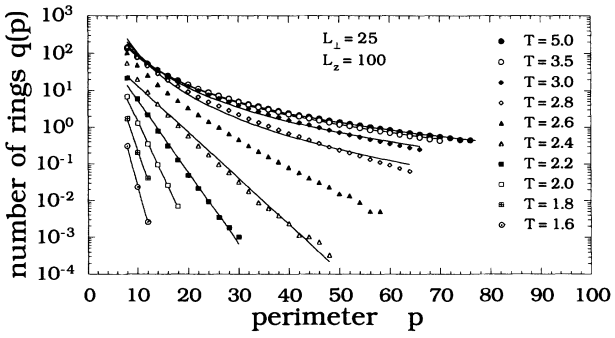


FIG. 14. Distribution of thermally excited closed vortex rings of perimeter $p$ versus $p$. Several different temperatures are shown for the fixed system size $L_\perp = 25$, $L_z = 100$. For $T < T_{cz} \simeq 2.6$ solid lines are the best fit to an exponential decay. For $T > T_{cz}$ solid lines are the best fit to an algebraic decay.

For low $T < T_{cz} \simeq 2.6$, we see an exponential decay $q(p) \sim \exp(-\varepsilon' p/T)$, consistent with the discussion above. Comparison with Eqs. (5) and (6) gives for the effective ring line tension, $\varepsilon'$, at low temperatures,

$$\varepsilon' = (1 - T/T_0)\varepsilon. \tag{7}$$

For larger $T > T_{cz}$, we see a slower than exponential decay, which is well fit by an algebraic power law, $q(p) \sim p^{-x}$, $x \simeq 2.56$, 2.69, 3.07, 3.75 for $T = 5.0$, 3.5, 3.0, 2.8, respectively. The crossover from exponential to algebraic decay occurs near $T_{cz}$. The transition at $T_{cz}$ can therefore be described as the vanishing of the ring line tension $\varepsilon'$ as $T$ increases to $T_{cz}$. This picture has some similarities with proposed vortex ring unbinding theories of the phase transition in the ordinary three-dimensional $XY$ model.[7]

### E. 2D boson analogy

As a final indication that $T_{cz}$ is a vortex percolation-like transition, we compute a quantity motivated by Nelson's analogy[4] between the field induced vortex lines of a superconductor, and the imaginary time world lines of two-dimensional bosons. According to this analogy, the 2D boson superfluid density $\rho_s$ is nonzero only when superconducting coherence parallel to the applied magnetic field is lost.[8–10] A convenient expression for $\rho_s$ has been given by Ceperley and Pollack[11] in terms of the "winding number" $\mathbf{W}$ of boson world lines, $\rho_s = mT_{\rm boson}\langle W^2\rangle/2\hbar^2$ where $T_{\rm boson}$ is the temperature of the boson system. The mapping[4] to the superconductor problem is given by $\hbar/T_{\rm boson} \to L_z$, $\hbar \to T_{\rm super}$, $m \to \epsilon_1 \sim \pi J_0$, the single vortex-line tension. Hence $\rho_s \sim \langle W^2\rangle/L_z$. The winding number is defined[11] in terms of the boson world lines, or equivalently in terms of the magnetic field induced vortex lines, as

$$\mathbf{W} = \frac{1}{L_\perp}\sum_{i=1}^{N_v}[\mathbf{r}_{\perp i}(L_z) - \mathbf{r}_{\perp i}(0)]. \tag{8}$$

$\mathbf{W}$ measures the net "winding" of the lines about the system in the $xy$ plane [$\mathbf{W}$ should not be confused with our earlier distribution $n(m)$ which measures winding of lines about the $\hat{\mathbf{z}}$ direction]. Since the periodic boundary condition along $\hat{\mathbf{z}}$ implies that the set of points $\{\mathbf{r}_{\perp i}(0)\}$ is equivalent to the set of points $\{\mathbf{r}_{\perp i}(L_z)\}$, $\mathbf{W}$ can be nonzero only if periodic boundary conditions also exist in the $\hat{\mathbf{x}}$ and $\hat{\mathbf{y}}$ directions. If we assume that the only vortex lines present in the system are the magnetic field induced lines, then $\mathbf{W}$ is just equal to the net vorticity in the directions perpendicular to the magnetic field, or equivalently the perpendicular part of the $q = 0$ Fourier transform of the vortex density $\mathbf{n}(\mathbf{r}_\perp, z) \equiv (1/2\pi)\boldsymbol{\nabla} \times \boldsymbol{\nabla}\theta$,

$$\mathbf{W} = \frac{1}{L_\perp}\mathbf{n}^\perp_{q=0} \equiv \frac{1}{L_\perp}[\mathbf{n}_{q=0} - \hat{\mathbf{z}}(\hat{\mathbf{z}}\cdot\mathbf{n}_{q=0})]. \tag{9}$$

Note a crucial difference between $\mathbf{n}_{q=0}$ and the line densities $\Delta l_\mu$ we defined earlier: $\Delta l_\mu$ measures the total length of vortex-line segments, independent of the direction of the vorticity; $\mathbf{n}_{q=0}$ measures net vorticity; i.e., two line segments oriented in opposite directions will cancel in their contribution to $\mathbf{n}_{q=0}$.

The Hamiltonian of our system Eq. (1) can be expressed[2] in terms of the vortex density as

$$\mathcal{H}[\mathbf{n}_q] = \frac{2\pi^2 J_0}{L_z L_\perp^2}\sum_q (\mathbf{n}_q - f\hat{\mathbf{z}}\delta_{q,0})\cdot(\mathbf{n}_q - f\hat{\mathbf{z}}\delta_{q,0})G_q, \tag{10}$$

where the interaction $G_q \sim 1/q^2$ as $q \to 0$. To keep the total energy finite, we are thus rigorously constrained in our model to configurations where $\mathbf{n}^\perp_{q=0} = 0$. Hence as long as we assume that the only vortex lines present in the system are the field induced lines, we must have $\mathbf{W} = 0$. If we now include the possibility of closed vortex ring excitations, the identification of Eq. (9) continues to be correct provided the rings remain of *finite* length $p$; the net vorticity of a finite ring always vanishes as the vorticity must always reverse direction in order for the ring to close back on itself. Only if we have rings so large (i.e., infinite as $L_\perp \to \infty$) that they wind completely around the system in the $\hat{\mathbf{x}}$ or $\hat{\mathbf{y}}$ direction, making use of the periodic boundary conditions to close back on themselves without ever reversing the direction of their vorticity, will the identification between $\mathbf{W}$ and $\mathbf{n}^\perp_{q=0}$ in Eq. (9) break down. A nonzero $\mathbf{W}$ computed as in Eq. (8) is now possible, provided its contribution to $\mathbf{n}^\perp_{q=0}$ is exactly canceled by an oppositely oriented contribution to $\mathbf{n}^\perp_{q=0}$ from the infinite transverse ring.

In Fig. 15 we plot $\langle W^2\rangle/L_z$ versus $T$ for system sizes $L_z = 100$, $L_\perp = 15$, 20, 25, and $L_z = 50$, $L_\perp = 25$. We see that $W^2$ is only nonzero above $T_{cz} \simeq 2.6$. Thus only above $T_{cz}$ do we find vortex rings that travel completely around the system in the direction transverse to the applied magnetic field. This is only possible once the vortex tangle, of interconnected magnetic field induced lines and thermally excited rings, percolates throughout the entire system. Note that our results for $\langle W^2\rangle/L_z$ show some difficulties with the interpretation of this quantity as a 2D boson superfluid density. Comparing sizes $L_\perp = 25$, $L_z = 50$, 100, we see no change in $\langle W^2\rangle/L_z$, even though different $L_z$ correspond to different temperatures $T_{\rm boson}/\hbar = 1/L_z$ in the 2D boson problem. For

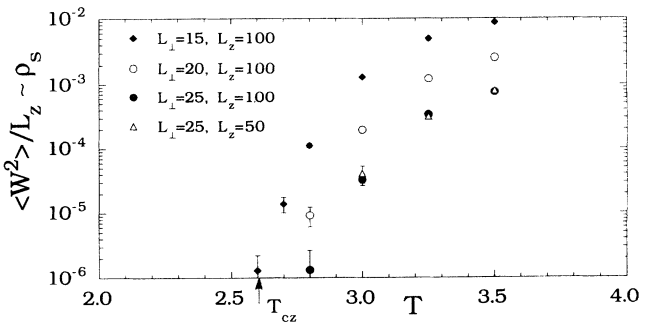


FIG. 15. Winding number $\langle W^2\rangle/L_z$ versus temperature for system sizes $L_z = 100$, $L_\perp = 15$, 20, 25, and $L_z = 50$, $L_\perp = 25$. $W^2 > 0$ only for $T > T_{cz} \simeq 2.6$.

fixed $L_z = 100$, and increasing $L_\perp$, we see a steady decrease in $\langle W^2 \rangle / L_z$ towards zero, in contrast to expectations that the 2D boson $\rho_s$ should approach a finite constant. We do not fully understand these size dependences. It has been suggested[9] that the results of Ceperley and Pollack for $\rho_s$ may not apply in the limit of a long range gauge interaction between 2D bosons, such as is the case in our superconductor problem. Nevertheless our results continue to support the view that $T_{cz}$ is a vortex percolation transition.

## IV. DISCUSSION

Although we have not tried in this work to model a particular high-$T_c$ copper oxide superconductor, it is worth indicating in what cases our results may qualitatively describe behavior in these materials. Our approximation of a uniform magnetic induction inside the material (formally equivalent to $\lambda \to \infty$) means our model should apply only in the limit where both the applied magnetic field is large enough[2] that $\lambda \gg a_v \sim \sqrt{\Phi_0/B}$, and the Josephson coupling between the CuO planes dominates[12] over the magnetic coupling, $\lambda_c < \lambda_{ab}^2/d$ (where $\lambda_c$, $\lambda_{ab}$ are the magnetic penetration lengths perpendicular to and within the CuO planes, respectively, and $d$ is the separation between the CuO planes). Behavior in the high-$T_c$ materials has been further characterized with reference to a critical magnetic field,[12–14] $B_{\rm cr} \simeq \Phi_0 \lambda_{ab}^2 / \lambda_c^2 d^2$. For $B < B_{\rm cr}$, vortices within different CuO planes may be thought of as correlated strings, an anisotropic Landau-Ginzburg description is adequate, and the melting of the vortex line lattice is "three dimensional." For $B > B_{\rm cr}$, vortices within different CuO planes are weakly coupled, the layered Lawrence-Doniach model[15] is more appropriate, and melting is "quasi-two-dimensional." Since in our simulation we have taken $J_0 \sim 1/\lambda^2$ constant in all directions, and the spacing between vortices is $a_v/a = 5$, if we identify the lattice constant of our numerical mesh $a$ with the spacing between CuO planes $d$, we have $\Phi_0/a_v^2 = B < B_{\rm cr}$ and our results apply in the region where melting is three dimensional.[16]

One of the primary results of this paper has been to substantiate the existence in our model of two separate phase transitions at $T_{c\perp}$ and $T_{cz}$. The transition at $T_{cz}$ implies the existence of two distinct vortex-line liquid states. Nelson[4] had originally suggested a similar transition, between an entangled and a disentangled line liquid, as a *finite size* effect when the entanglement length $\xi_z \approx L_z$. However, as our measured $\Upsilon_z$ shows no dependence at all on $L_z$ (except very close to $T_{cz}$), no hysteresis on heating versus cooling, and no dependence on the degree to which the low-temperature state is entangled, we rule out such finite size effects as the origin of our transition at $T_{cz}$. In particular, using our earlier results from (I) (see Fig. 5 of Ref. 2), we find that at least for the region $2.2 < T < T_{cz}$, $\xi_z < 10$ remains many times smaller than our largest system size $L_z = 200$.

At the lower transition $T_{c\perp}$, the vortex-line lattice melts upon heating [see (I)], $\Upsilon_\perp \to 0$, and superconducting coherence is lost in the planes perpendicular to the applied magnetic field. At the upper transition $T_{cz}$, a vortex tangle percolates completely through the system in the directions transverse to the applied magnetic field, $\Upsilon_z \to 0$, and superconducting coherence is lost in the direction parallel to the magnetic field. Identifying the loss of superconducting coherence with the onset of linear electric resistivity, we therefore would expect the following experimental consequences: As $T$ is decreased, the linear resistivity for currents applied parallel to the magnetic field will vanish below $T_{cz}$. However, linear resistivity for currents applied perpendicular to the magnetic field will continue to remain finite below $T_{cz}$ until a lower $T_{c\perp}$ is reached. This result is in precise agreement with earlier predictions by Feigel'man and co-workers,[8,9] who work within the two-dimensional boson approximation; similar behavior has been suggested by Glazman and Koshelev[12] for $B < B_{\rm cr}$.

Recent experiments[17] by Steel, White, and Graybeal on synthetic MoGe/Ge multilayers appear to show precisely such behavior. In these experiments, in which the magnetic field is applied perpendicular to the layers, the authors observe a well-defined temperature "$T_D$" at which the resistivity parallel to the magnetic field shows a dramatic drop, accompanied by the onset of substantial nonlinearities in the $I$-$V$ characteristics. This suggests a transition where the linear resistivity in this direction vanishes. The resistivity perpendicular to the magnetic field shows a kink at $T_D$, however, continues to remain linear for temperatures $T < T_D$. Such behavior is consistent with that of our middle phase $T_{c\perp} < T < T_{cz}$, if we identify the experimental $T_D$ with our $T_{cz}$. These experiments however appear to be in the region $B > B_{\rm cr}$, and so the direct application of our results remains unclear.

A second important result of our paper has been the observation that upon cooling below $T_{cz}$, lines can get trapped in a disordered entangled state where vortex-line cutting is frozen out except on long time scales. Here the disorder is purely topological in nature[5] and not due to any random impurities. The importance of such entanglement on transport properties determined by vortex-line diffusion, has been stressed by Nelson and co-workers,[4,18] particularly with regard to pinning by large scale impurities.

Finally, we have identified the upper transition of our model, $T_{cz}$, as the temperature at which an interconnected tangle of wandering vortex lines and thermally excited vortex rings percolates through the system. Our analysis of the vortex ring distribution suggests that this is the temperature at which the effective vortex-line tension vanishes. Since a vortex line may qualitatively be viewed as a one-dimensional "interface" between different ground states of the 3D $XY$ model, the two transitions of our model might be viewed in analogy to the behavior of interfaces in the 3D Ising model. Our lower melting transition $T_{c\perp}$ might be viewed like a "roughening" transition. Below $T_{c\perp}$ lines remain straight as $L_z \to \infty$, and are periodically ordered. Above $T_{c\perp}$ line wandering increases with increasing $L_z$, and lines are disordered in the plane; however, lines retain a finite line tension and so remain well-defined fluctuating objects. Our upper transition $T_{cz}$ might be viewed as the "bulk" transition

where the effective line tension vanishes, and detached "bubbles," i.e., vortex rings, proliferate. A similar picture is implied in work by Bulaevskii *et al.*[19] and by Glazman and Koshelev.[12]

In our discussion of the 2D boson analogy in Sec. III E, we derived the important consequence that $\rho_s \equiv 0$ for all $T$ below the vortex percolation transition, from the observation that the vortex-line interaction of our model[2] was $G_q \sim 1/q^2$, and hence energy conservation strictly requires $\mathbf{W} \sim \mathbf{n}^{\perp}_{q=0} = 0$. This is a direct consequence of our approximation $\lambda \to \infty$. For finite $\lambda$, the interaction[2] is $G_q \sim 1/(q^2 + \lambda^{-2})$, and now fluctuations with finite $\mathbf{n}^{\perp}_{q=0} > 0$ are energetically possible in the vortex-line liquid phase. This could imply finite $\rho_s$, and vanishing superconducting coherence along the direction of the magnetic field. Recent work by Chen and Teitel,[10] however, suggests that, for finite $\lambda$, superconducting coherence along the magnetic field may still persist in a hexatic vortex-line liquid state,[20] which might exist intermediate to the vortex-line lattice, and normal vortex-line liquid states. In this case, it remains to be seen if the hexatic to normal line liquid transition coincides with the vortex percolation transition of our model, or if the vortex percolation remains a sharp thermodynamic transition at all. Even if a finite $\lambda$ should turn out to destroy the sharp transition we find at $T_{cz}$, our results may still apply in the limit of a sample of thickness $d < \lambda$ (as in the experiments of Ref. 17), and should indicate the existence of a strong crossover region in thicker samples.

## ACKNOWLEDGMENTS

It is a pleasure to thank Professor D. R. Nelson, Professor M. V. Feigel'man, Professor D. S. Fisher, and Professor J. M. Graybeal for helpful conversations. This work has been supported by U.S. Department of Energy Grant No. DE-FG02-89ER14017.

* Present address: Department of Physics and Astronomy, University of Rochestere, Rochester, NY 14627.

[1] Y.-H. Li and S. Teitel, Phys. Rev. Lett. **66**, 3301 (1991); Phys. Rev. B **45**, 5718 (1992).

[2] Y.-H. Li and S. Teitel, Phys. Rev. B **47**, 359 (1993).

[3] See also R. E. Hetzel, A. Sudbø, and D. A. Huse, Phys. Rev. Lett. **69**, 518 (1992); R. Cavalcanti, G. Carneiro, and A. Gartner, Europhys. Lett. **17**, 449 (1992); G. Carneiro, R. Cavalcanti, and A. Gartner, Phys. Rev. B **47**, 5263 (1993).

[4] D. R. Nelson, Phys. Rev. Lett. **60**, 1973 (1988); J. Stat. Phys. **57**, 511 (1989); D. R. Nelson and H. S. Seung, Phys. Rev. B **39**, 9153 (1989); D. R. Nelson and P. LeDoussal, *ibid.* **42**, 10 113 (1990).

[5] S. P. Obukhov and M. Rubinstein, Phys. Rev. Lett. **65**, 1279 (1990); **66**, 2279 (1991).

[6] An interesting distinction between the use of free versus periodic boundary conditions for physical samples of *finite* width has been made in M. P. A. Fisher and D. H. Lee, Phys. Rev. B **39**, 2756 (1989). However, this distinction vanishes in the thermodynamic limit of infinite thickness. Since we view our numerical system of finite width $L_z$ as representing a region in the interior of an infinite bulk sample, and we are interested only in the limit of asymptotically large $L_z$, our use of periodic boundary conditions poses no special concerns.

[7] S. R. Shenoy, Phys. Rev. B **40**, 5056 (1989); B. Chattopadhyay, M. C. Mahato, and S. R. Shenoy, *ibid.* **47**, 15 159 (1993).

[8] M. V. Feigel'man, Physica A **168**, 319 (1990); M. V. Feigel'man, V. B. Geshkenbein, and V. M. Vinokur, Pis'ma Zh. Eksp. Teor. Fiz. **52**, 1141 (1990) [JETP Lett. **52**, 546 (1990)].

[9] M. V. Feigel'man, V. B. Geshkenbein, L. B. Ioffe, and A. I. Larkin (unpublished); M. V. Feigel'man (private communication).

[10] T. Chen and S. Teitel (unpublished).

[11] D. M. Ceperley and E. L. Pollock, Phys. Rev. B **36**, 8343 (1987).

[12] L. I. Glazman and A. E. Koshelev, Phys. Rev. B **43**, 2835 (1991).

[13] M. V. Feigel'man, V. B. Geshkenbein, and A. I. Larkin, Physica C **167**, 177 (1990).

[14] D. S. Fisher, M. P. A. Fisher, and D. A. Huse, Phys. Rev. B **43**, 130 (1991).

[15] W. E. Lawrence and S. Doniach, in *Proceedings of the International Conference on Low Temperature Physics, LT-12*, Kyoto, 1970, edited by E. Kanda (Keigaku, Tokyo, 1971), p. 361.

[16] The comment to the contrary in Ref. 36 of (I) is in error.

[17] D. G. Steel, W. R. White, and J. M. Graybeal, Phys. Rev. Lett. **71**, 161 (1993).

[18] M. C. Marchetti and D. R. Nelson, Phys. Rev. B **42**, 9938 (1990); Physica C **174**, 40 (1991).

[19] L. N. Bulaevskii, M. Ledvij, and V. G. Kogan, Phys. Rev. Lett. **68**, 3773 (1992); L. N. Bulaevskii, S. V. Meshkov, and D. Feinberg, Phys. Rev. B **43**, 3728 (1991).

[20] M. C. Marchetti and D. R. Nelson, Phys. Rev. B **41**, 1910 (1990).